MTPA Control of IPMSM Drives Based on Virtual Signal Injection Considering Machine Parameter Variations

Tianfu Sun, *Member, IEEE*, Mikail Koç, and Jiabin Wang, *Senior Member, IEEE*

***Abstract*—Due to parameter variations with stator currents, the derivatives of machine parameters with respect to current angle or *d*-axis current are not zero. However, these derivative terms are ignored by most of mathematical model based efficiency optimized control schemes. Therefore, even though the accurate machine parameters are known, these control schemes cannot calculate the accurate efficiency optimized operation points. In this paper, the influence of these derivative terms on maximum torque per ampere (MTPA) control is analyzed and a method to take into account these derivative terms for MTPA operation is proposed based on the recently reported virtual signal injection control (VSIC) method for interior permanent magnet synchronous machine (IPMSM) drives. The proposed control method is demonstrated by both simulations and experiments under various operating conditions on prototype IPMSM drive systems.**

***Index Terms*—Interior permanent magnet synchronous machine (IPMSM) drives, maximum torque per ampere (MTPA), parameter variation, virtual signal injection control (VSIC).**

I. Introduction

THE interior permanent magnet synchronous machines (IPMSM) have the advantages of high efficiency, high power density, and wide constant power operating range [1]. In order to achieve the efficiency optimal control of IPMSM drives, the maximum torque per ampere control (MTPA) scheme was proposed [2]–[4]. However, the IPMSMs are well known for their machine parameter uncertainty and nonlinear characteristics due to the high level of magnetic saturation, cross-coupling effects, and parameter dependency on temperature [5]. Therefore, to achieve the accurate MTPA operation is one of the significant challenges associated with the IPMSM control techniques and a large number of studies have been reported in the literature to improve the efficiency of the IPMSM drives. The state-of-the-art MTPA control schemes for IPMSM drives reported in literature can be classified broadly into three categories, i.e., lookup table based methods [6]–[8], the mathematical model based techniques [4], and the online search based techniques [9], which also include the signal injection based techniques [10]–[13].

The lookup table based methods are a kind of widely adopted MTPA control schemes which require relatively low computational load. The data in lookup tables can be obtained from a set of experiments [6] or from numerical analysis of electromagnetic field of the machine under consideration [8]. However, either the experiments or numerical analysis are time consuming and require considerable resources. More importantly, the accuracy of such control schemes cannot be guaranteed due to the manufacture tolerance, material property variations, and temperature influence.

The mathematical model based MTPA control schemes are another kind of widely adopted MTPA control schemes which utilize the inherent characteristic of the MTPA operation, i.e., the partial derivative of torque with respect to the current angle equals zero, to calculate the MTPA operation points online based on the mathematical model and machine parameters [3], [4]. The machine parameters can be obtained from lookup tables [8], [14] or from the online parameter estimations [15]–[19]. However, as discussed in [20], most of these kinds of control schemes do not fully consider the machine parameter variations, i.e., ignoring the derivatives of machine parameters with respect to the current angle or *d*-axis current. Therefore, even though the accurate machine parameters can be known, these MTPA control schemes cannot accurately calculate the MTPA operation point and the deviation from the optimal increases with the load. This problem, indeed, is the main concern of this paper and it will be clarified and addressed in great detail.

Instead of online calculation, the online-search-based MTPA control schemes [9], including the signal injection based MTPA control schemes [10]–[13], adjust the current vector through perturbation until the MTPA condition is met for a given torque command. These MTPA control schemes are independent of machine parameters but need to inject perturbations into

Manuscript received July 26, 2017; revised October 16, 2017 and November 17, 2017; accepted December 3, 2017. Date of publication December 18, 2017; date of current version April 2, 2018. *(Corresponding author: Mikail Koç.)*

T. Sun was with the University of Sheffield, Sheffield S1 3JD, U.K. He is now with the Shenzhen Institutes of Advanced Technology, Chinese Academy of Sciences, Shenzhen 100864, China (e-mail: tianfu.sun@foxmail.com).

M. Koç was with the University of Sheffield, Sheffield S1 3JD, U.K. He is now with Ahi Evran University, Kirsehir 40100, Turkey (e-mail: mkoc@ahievran.edu.tr).

J. Wang is with the Department of Electronic and Electrical Engineering, University of Sheffield, Sheffield S1 3JD, U.K. (e-mail: j.b.wang@sheffield.ac.uk).

Color versions of one or more of the figures in this paper are available online at http://ieeexplore.ieee.org.

Digital Object Identifier 10.1109/TIE.2017.2784409

0278-0046 © 2017 IEEE. Personal use is permitted, but republication/redistribution requires IEEE permission.
See http://www.ieee.org/publications_standards/publications/rights/index.html for more information.

Authorized licensed use limited to: ULAKBIM-UASL - Ahi Evran Universitesi. Downloaded on March 16,2022 at 12:48:36 UTC from IEEE Xplore. Restrictions apply.

current vector or voltage vector. The perturbations will cause additional losses and harmonics which will deteriorate control performance and greatly limit the scope of this kind of approaches for the MTPA operation.

Recently, virtual signal injection control was proposed to track the MTPA points by injecting high-frequency signal into the IPMSM torque equation mathematically [21]–[23]. Since the VSIC scheme does not inject any real signal into motor, therefore, the additional power losses, increased current/voltage harmonics, and the resonant problems associated with the real signal injection are inherently avoided. The accuracy of virtual signal injection based MTPA control is analyzed in [20] and two forms of torque equations for injecting virtual signals are proposed. As discussed in [20], by proper selecting the form of the torque equation, the error of MTPA control due to the neglect of the derivatives of machine parameters with respect to current angle or d-axis current can be partly canceled. However, the selection of the equation depends on machine characteristics [20] and the accuracy of virtual signal injection based MTPA control may vary with different motors and operation conditions.

In this paper, a compensation scheme that can compensate the error due to the neglect of the derivative of machine parameters with respect to current angle is proposed based on the virtual signal injection concept. The proposed control scheme is verified by simulations and experiments. It is shown that the proposed control scheme can compensate the error effectively and can achieve relatively high MTPA control accuracy.

II. Influences of Machine Parameter Variation

The mathematical model of a three-phase IPMSM in d-q reference frame with sinusoidal stator current excitation is shown in (1) to (3) as follows:

$$v_q = L_q \frac{di_q}{dt} + Ri_q + p\,\omega_m L_d i_d + p\,\omega_m \Psi_m \tag{1}$$

$$v_d = L_d \frac{di_d}{dt} + Ri_d - p\,\omega_m L_q i_q \tag{2}$$

$$T_e = \frac{3p}{2}\left[\Psi_m i_q + (L_d - L_q)\, i_d i_q\right] \tag{3}$$

$$i_d = -I_a \sin(\beta) \quad i_q = I_a \cos(\beta) \tag{4}$$

where v_d and v_q are the d- and q-axis voltages, respectively. The d-axis inductance L_d, the q-axis inductance L_q, and the permanent magnet flux linkage Ψ_m are the functions of both d-axis current i_d and q-axis current i_q due to the magnetic saturation effect. p is the number of pole-pairs and ω_m is the rotor speed. I_a and β denote the current amplitude and the current angle with respect to the q-axis, respectively.

According to (3) and (4), the derivative of torque with respect to current angle ($\partial T_e/\partial\beta$) is expressed as follows:

$$\frac{\partial T_e}{\partial \beta} = \frac{3p}{2}\left[-\Psi_m I_a \sin\beta + \frac{\partial \Psi_m}{\partial \beta} I_a \cos\beta - L_d I_a^2 \cos 2\beta + L_q I_a^2 \cos 2\beta - \frac{\partial L_d}{\partial \beta}\frac{I_a^2}{2}\sin 2\beta + \frac{\partial L_q}{\partial \beta}\frac{I_a^2}{2}\sin 2\beta\right]. \tag{5}$$

TABLE I
Parameters of the First IPMSM Model

Number of pole-pairs	3
Phase resistance	51.2 mΩ
Maximum current	118 A
Peak power below base speed	10 kW
Base/maximum speed	1350/4500 r/min
Continuous/peak torque	35.5/70 N·m
Nominal d-axis inductance	0.71 mH
Nominal q-axis inductance	1.94 mH
Nominal permanent magnet flux linkage	112.1 mWb
Peak power at maximum speed	7 kW

By ignoring the derivatives of machine parameters with respect to current angle ($\partial\Psi_m/\partial\beta$, $\partial L_d/\partial\beta$, $\partial L_q/\partial\beta$), the well-known mathematical model of MTPA curves [24] given by the following equations is derived [3], [4]. They have been employed in IPMSM drives extensively [25]

$$i_d = \frac{\Psi_m}{2\,(L_q - L_d)} - \sqrt{\frac{\Psi_m^2}{4(L_q - L_d)^2} + i_q^2} \tag{6}$$

$$\beta = \sin^{-1}\frac{-\Psi_m + \sqrt{{\Psi_m}^2 + 8(L_q - L_d)^2 {I_a}^2}}{4\,(L_q - L_d)\, I_a}. \tag{7}$$

However, it is highly important to note that even though the machine parameters employed in (6) and (7) are accurate, precise MTPA operation still cannot be achieved. This is due to the neglect of the derivative terms ($\partial\Psi_m/\partial\beta$, $\partial L_d/\partial\beta$, $\partial L_q/\partial\beta$) in (5). The influence of these derivatives in (5), namely, $I_a \cos\beta\partial\Psi_m/\partial\beta$, $-I_a^2 \sin 2\beta(\partial L_d/\partial\beta)/2$, $I_a^2 \sin 2\beta(\partial L_q/\partial\beta)/2$ increases with load or current amplitude I_a. Therefore, when the current amplitude I_a is relatively large, the influence of these derivation terms would be significant around the MTPA points ($\partial T_e/\partial\beta = 0$).

In order to study the influence of these derivative terms, simulations were performed based on a nonlinear IPMSM machine developed for distributed traction of a microsize electric vehicle with peak power of 10 kW at the base speed of 1350 r/min. The machine specifications are given in Table I. During the simulation, the current angle (β) varied from 20° to 45° with current amplitude equal to 80 A. The derivative terms $3pI_a \cos\beta(\partial\Psi_m/\partial\beta)/2$, $-3pI_a^2 \sin 2\beta(\partial L_d/\partial\beta)/4$, and $3pI_a^2 \sin 2\beta(\partial L_q/\partial\beta)/4$ in (5) are compared with $\partial T_e/\partial\beta$ and shown in Fig. 1. The "$\mathrm{error_{MTPA}}$" in Fig. 1 is the sum of the derivative terms and given by the following equation:

$$\begin{aligned}\mathrm{error_{MTPA}} &= \frac{3p}{2}\left[\frac{\partial\Psi_m}{\partial\beta} I_a \cos\beta - \frac{\partial L_d}{\partial\beta}\frac{I_a^2}{2}\sin 2\beta + \frac{\partial L_q}{\partial\beta}\frac{I_a^2}{2}\sin 2\beta\right] \\ &= \frac{3p}{2}\left[\frac{\partial\Psi_m}{\partial\beta} + \frac{\partial L_d}{\partial\beta} i_d - \frac{\partial L_q}{\partial\beta} i_d\right] i_q.\end{aligned} \tag{8}$$

As shown in Fig. 1, the real MTPA point is the point where $\partial T_e/\partial\beta = 0$. However, if the derivative terms in (5) are ignored, the resultant MTPA point with error will be the

Authorized licensed use limited to: ULAKBIM-UASL - Ahi Evran Universitesi. Downloaded on March 16,2022 at 12:48:36 UTC from IEEE Xplore. Restrictions apply.

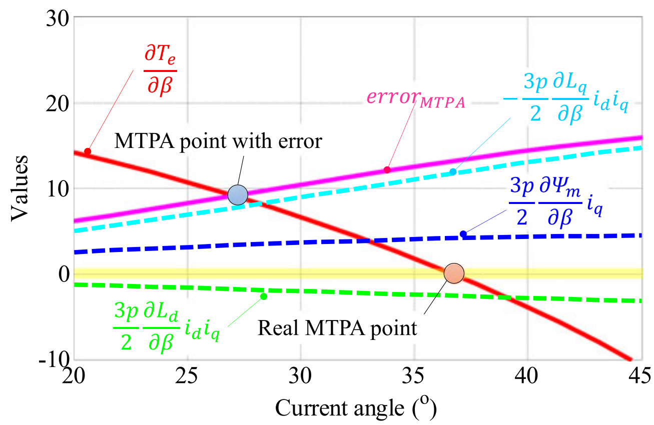

Fig. 1. Comparison of the derivative terms with $\partial T_e/\partial \beta$.

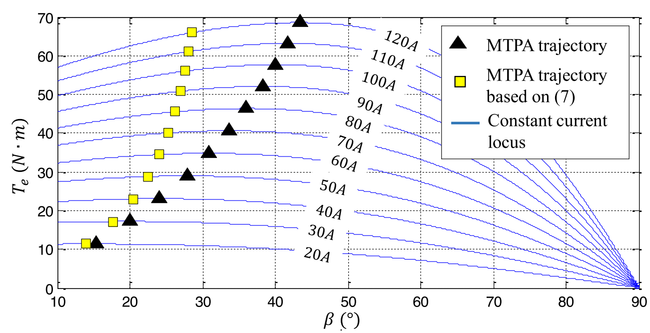

Fig. 2. Torque versus current angle of the real MTPA points and the MTPA points calculated by (7).

intersection of the $\partial T_e/\partial \beta$ curve and the $\mathrm{error}_{\mathrm{MTPA}}$ curve, i.e., $\partial T_e/\partial \beta - \mathrm{error}_{\mathrm{MTPA}} = 0$. The current angle corresponding to the real MTPA point is about 36.7°, however, the current angle of resultant MTPA point when the derivative terms are ignored is about 27.1°, resulting in about 35% error in the current angle! This error will be greater as the current amplitude increases.

To illustrate the influence of the derivative terms on MTPA control, constant current loci for every 10 A from 20 to 120 A (the maximum current amplitude of the motor) together with the real MTPA points and the resultant MTPA points calculated by (7), i.e., when the derivative terms are ignored, are shown in Fig. 2. The machine parameters in (7) are the same as the machine parameters in the nonlinear motor model.

As can be seen in Fig. 2, due to the derivative terms, although the machine parameters in (7) are accurate, the errors of MTPA control based on (6) and (7) are still significant.

III. Virtual Signal Injection Based Control Scheme for MTPA Operation

A. Principle of Virtual Signal Injection

The virtual signal injection based control schemes for MTPA operation have been reported in recent years [20]–[22]. This kind of control schemes can track the MTPA points online without injecting any real signals into motor. The VSIC schemes can

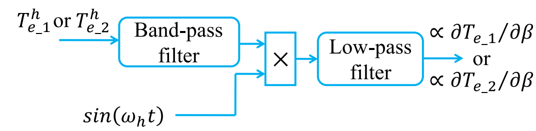

Fig. 3. Signal processing scheme.

be realized by the equations given in (9) and (10), respectively, depending on the characteristics of the motor [20]:

$$T^h_{e\_1} = \frac{3p}{2}\left\{\frac{v_q - Ri_q}{p\,\omega_m} - L_d\left(i_d - i^h_d\right) + \frac{v_d - Ri_d}{p\,\omega_m i_q} i^h_d\right\} i^h_q \tag{9}$$

$$T^h_{e\_2} = \frac{3p}{2}\left[\frac{(v_q - Ri_q)}{\omega_m} + \frac{(v_d - Ri_d)}{i_q \omega_m} i^h_d\right] i^h_q \tag{10}$$

where

$$i^h_d = -I_a \sin(\beta + \Delta\beta) \tag{11}$$

$$i^h_q = I_a \cos(\beta + \Delta\beta) \tag{12}$$

$$\Delta\beta = A \sin(\omega_h t) \tag{13}$$

where ω_h is the angular frequency of the perturbation injected into the d- and q-axis currents mathematically. According to (9) and (10), the resultant calculated torque perturbation $T^h_{e\_1}$ and $T^h_{e\_2}$ can be calculated based on the measured d- and q-axis currents, the reference d- and q-axis voltages, the rotor speed, and the nominal stator resistances mathematically. L_d in (9) can be assumed to its nominal value or obtained from a lookup table.

As described in [22] and [26], based on Taylor's series expansion, the left-hand side of (9) and (10) can be expressed as the following equations, respectively

$$T^h_{e\_1} = T_{e\_1}(\beta + A\sin(\omega_h t)) = T_{e\_1}(\beta) + \frac{\partial T_{e\_1}}{\partial \beta} A \sin(\omega_h t) + \frac{\partial}{2\partial \beta}\left(\frac{\partial T_{e\_1}}{\partial \beta}\right) A^2 \sin^2(\omega_h t) + \ldots \tag{14}$$

$$T^h_{e\_2} = T_{e\_2}(\beta + A\sin(\omega_h t)) = T_{e\_2}(\beta) + \frac{\partial T_{e\_2}}{\partial \beta} A \sin(\omega_h t) + \frac{\partial}{2\partial \beta}\left(\frac{\partial T_{e\_2}}{\partial \beta}\right) A^2 \sin^2(\omega_h t) + \ldots. \tag{15}$$

According to (14) and (15), $T^h_{e\_1}$ and $T^h_{e\_2}$ contain the information of $\partial T_{e\_1}/\partial \beta$ and $\partial T_{e\_2}/\partial \beta$, respectively. Thus, the information of $\partial T_{e\_1}/\partial \beta$ or $\partial T_{e\_2}/\partial \beta$ can be extracted by the signal processing scheme shown in Fig. 3. The center frequency of the bandpass filter in Fig. 3 equals the virtually injected signal frequency (ω_h) to eliminate other higher order terms in (14) or (15).

The output of the bandpass filter will be multiplied by $\sin(\omega_h t)$ and the result is given in (16) or (17), where K is

Authorized licensed use limited to: ULAKBIM-UASL - Ahi Evran Universitesi. Downloaded on March 16,2022 at 12:48:36 UTC from IEEE Xplore. Restrictions apply.

the gain of the bandpass filter at ω_h

$$K\frac{\partial T_{e\_1}}{\partial \beta}A\sin^2(\omega_h t) = K\frac{\partial T_{e\_1}}{\partial \beta}A\left\{\frac{1}{2}\left[\cos(0)-\cos(2\omega_h t)\right]\right\} = \frac{1}{2}KA\frac{\partial T_{e\_1}}{\partial \beta} - \frac{\partial T_{e\_1}}{\partial \beta}KA\cos(2\omega_h t) \tag{16}$$

$$K\frac{\partial T_{e\_2}}{\partial \beta}A\sin^2(\omega_h t) = K\frac{\partial T_{e\_2}}{\partial \beta}A\left\{\frac{1}{2}\left[\cos(0)-\cos(2\omega_h t)\right]\right\} = \frac{1}{2}KA\frac{\partial T_{e\_2}}{\partial \beta} - \frac{\partial T_{e\_2}}{\partial \beta}KA\cos(2\omega_h t). \tag{17}$$

The right-hand side of (16) or (17) will be filtered by a first-order low-pass filter whose cutoff frequency is below the virtually injected signal frequency ω_h to obtain the signal proportional to $\partial T_{e\_1}/\partial\beta$ or $\partial T_{e\_2}/\partial\beta$. The output of the low-pass filter will be utilized to adjust the reference *d*-axis current or the reference current angle until it equals zero. In this way, the MTPA points can be approached [20].

B. Error Analysis

In steady state, by the substitution of (1), (2), and (4) into (9) and (10), the derivatives of T_{e_1} and T_{e_2} with respect to the current angle can be deduced in (18) and (19), respectively. It is worth noting that since $\Delta\beta$ in (11) and (12) is injected mathematically and no real signal is injected into motor, the measured *d*- and *q*-axis currents and the reference *d*- and *q*-axis voltages will not vary with $\Delta\beta$, nor do the machine parameters in (18) and (19). Therefore, the output of the signal processing unit that is proportional to $\partial T_{e\_1}/\partial\beta$ or $\partial T_{e\_2}/\partial\beta$ also does not contain the derivative terms of the machine parameters with respect to β

$$\frac{\partial T_{e\_1}}{\partial \beta} = \frac{3p}{2}\left[-\Psi_m I_a\sin\beta - L_d I_a^2\cos 2\beta + L_q I_a^2\cos 2\beta\right] \tag{18}$$

$$\frac{\partial T_{e\_2}}{\partial \beta} = \frac{3p}{2}\Big[-\Psi_m I_a\sin\beta + L_d\frac{I_a^2}{2}(1-\cos 2\beta) + L_q I_a^2\cos 2\beta\Big]. \tag{19}$$

Comparison of (5) with (18) yields

$$\frac{\partial T_{e\_1}}{\partial \beta} = \frac{\partial T_e}{\partial \beta} - \mathrm{error}_1. \tag{20}$$

Comparison of (5) with (19) yields

$$\frac{\partial T_{e\_2}}{\partial \beta} = \frac{\partial T_e}{\partial \beta} - \mathrm{error}_2 \tag{21}$$

where

$$\mathrm{error}_1 = \frac{3p}{2}\left[\frac{\partial \Psi_m}{\partial \beta} + \frac{\partial L_d}{\partial \beta}i_d - \frac{\partial L_q}{\partial \beta}i_d\right]i_q = \mathrm{error}_{\mathrm{MTPA}} \tag{22}$$

$$\mathrm{error}_2 = \frac{3p}{2}\left[\frac{\partial \Psi_m}{\partial \beta} + \frac{\partial L_d}{\partial \beta}i_d - \frac{\partial L_q}{\partial \beta}i_d - L_d i_q\right]i_q. \tag{23}$$

Since

$$\frac{\partial \Psi_d}{\partial \beta} = \frac{\partial(\Psi_m + L_d i_d)}{\partial \beta} = \frac{\partial \Psi_m}{\partial \beta} + \frac{\partial L_d}{\partial \beta}i_d + L_d\frac{\partial i_d}{\partial \beta} \tag{24}$$

$$\frac{\partial i_d}{\partial \beta} = \frac{\partial(-I_a\sin(\beta))}{\partial \beta} = -I_a\cos(\beta) = -i_q. \tag{25}$$

Substitution of (24) and (25) into (23) yields

$$\mathrm{error}_2 = \frac{3p}{2}\left[-\frac{\partial L_q}{\partial \beta}i_d + \frac{\partial \Psi_d}{\partial \beta}\right]i_q. \tag{26}$$

According to (22), the virtual signal injection MTPA control based on (9) is equivalent to the conventional methods which are based on (6) and (7). However, only L_d is needed.

According to (26), for the motors that $i_d\partial L_q/\partial\beta$ is close to $\partial\Psi_d/\partial\beta$, the error_2 in (26) may be partly cancelled. In this case the MTPA control of the VSIC based on (10) may achieve better control accuracy than the virtual signal injection based on (9) and the methods based on (6) and (7). However, this is dependent on the characteristic of the motor. More details can be found in [20].

IV. Proposed Control Scheme

As discussed in Sections II and III, the MTPA control accuracy of the conventional MTPA control schemes based on (6) and (7), and the existing VSIC may be affected by the derivatives of machine parameters with respect to current angle. In order to compensate the error terms, the characteristics of the terms in (8) was studied.

For most IPMSMs, Ψ_m is the no-load *d*-axis flux linkage. According to (24), the variation of Ψ_d with respect to β should be dominated by the variation of *d*-axis current, i.e., $L_d\partial i_d/\partial\beta$ term in (24). Moreover, since the signs of $\partial\Psi_m/\partial\beta$ and $i_d\partial L_d/\partial\beta$ in (24) are opposite, $\partial\Psi_m/\partial\beta$ and $i_d\partial L_d/\partial\beta$ will partly cancel each other. Therefore, the sum of $\partial\Psi_m/\partial\beta$ and $i_d\partial L_d/\partial\beta$ in (8) should be relatively small and the "$\mathrm{error}_{\mathrm{MTPA}}$" given by (8) should be dominated by $-3pi_d i_q(\partial L_q/\partial\beta)/2$, as shown in Fig. 1. Consequently, the error due to neglect of the derivatives of machine parameters with respect to current angel can be effectively minimized by the compensation of $-3pi_d i_q(\partial L_q/\partial\beta)/2$ in (8).

The compensation of $-3pi_d i_q(\partial L_q/\partial\beta)/2$ requires the information of $\partial L_q/\partial\beta$. In order to extract the information of $\partial L_q/\partial\beta$, the knowledge of *q*-axis flux linkage (Ψ_q) is needed. The relationship between Ψ_q and *d*-axis voltage is given as

$$v_d = \frac{d\Psi_d}{dt} + Ri_d - p\omega_m\Psi_q. \tag{27}$$

Since the MTPA control only considers steady-state operation, the transient term $(d\Psi_d/dt)$ in (27) is ignored and the *q*-axis flux linkage can be estimated by the following equation through experiments or be calculated by the finite element analysis (FEA)

$$\Psi_q = -\frac{v_d - Ri_d}{p\omega_m}. \tag{28}$$

After Ψ_q is mapped with respect to *d*- and *q*-axis currents, it can be modeled as an *N*-order polynomial in the following

Authorized licensed use limited to: ULAKBIM-UASL - Ahi Evran Universitesi. Downloaded on March 16,2022 at 12:48:36 UTC from IEEE Xplore. Restrictions apply.

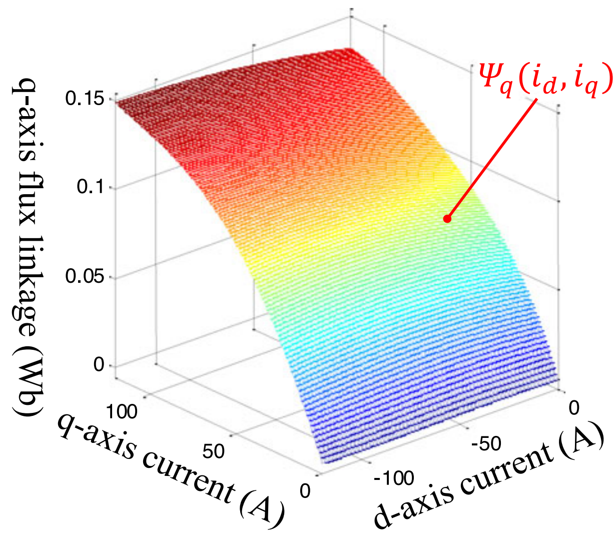

Fig. 4. *Q*-axis flux linkage (Ψ_q) as a polynomial of *d*- and *q*-axis currents.

equation:

$$\Psi_q(i_d, i_q) = \sum_{n=0}^{N} a_n i_d^n i_q^{N-n} \tag{29}$$

where a_n is the coefficients of the polynomial. In this paper, $\Psi_q(i_d, i_q)$ is mapped based on FEA data and a fifth-order polynomial is adopted to approximate Ψ_q since it yields satisfactory accuracy with manageable computation. The fitted $\Psi_q(i_d, i_q)$ map is shown in Fig. 4.

Since $L_q = \Psi_q(i_d, i_q)/i_q$, if $\Delta\beta$ in (13) is injected into the current angle, i.e., substitution of (11) and (12) into (29), the resultant *q*-axis inductance with the high-frequency component can be expressed as follows:

$$L_q^h(\beta + \Delta\beta) = \frac{\Psi_q\left(i_d^h, i_q^h\right)}{i_q^h}. \tag{30}$$

Based on Taylor's series expansion, the left-hand side of (30) can be expressed as follows:

$$\begin{aligned} L_q^h &= L_q(\beta + A\sin(\omega_h t)) \\ &= L_q(\beta) + \frac{\partial L_q}{\partial \beta} A \sin(\omega_h t) \\ &\quad + \frac{\partial}{2\partial\beta}\left(\frac{\partial L_q}{\partial\beta}\right) A^2 \sin^2(\omega_h t) + \ldots . \end{aligned} \tag{31}$$

Similar to the extraction of $\partial T_{e\_1}/\partial\beta$ and $\partial T_{e\_2}/\partial\beta$, the information of $\partial L_q/\partial\beta$ can be extracted by the signal processing scheme shown in Fig. 3. It is worth noting that the information of $\partial\Psi_m/\partial\beta$ and $\partial L_d/\partial\beta$ in $\text{error}_{\text{MTPA}}$ can also be extracted by the same method. However, this increases the complexity of the control scheme and requires more information about machine parameters.

Since the extraction of the information of $\partial T_{e\_1}/\partial\beta$ and $\partial L_q/\partial\beta$ are based on the same signal processing scheme, they are combined together and shown in Fig. 5.

Fig. 5 shows the schematic of virtual signal injection blocks for the generation of reference *d*-axis current for MTPA operation. The measured *d*- and *q*-axis currents are transformed into the polar coordinate system to calculate the current amplitude I_a and the current angle β. The high-frequency signal $\Delta\beta = A\sin(\omega_h t)$ is injected into the current angle β mathematically. The resultant *d*- and *q*-axis currents with high-frequency components i_d^h and i_q^h are calculated by (11) and (12). Then, the i_d^h and i_q^h are further fed into $\Psi_q(i_d, i_q)$ to generate the *q*-axis inductance with the high-frequency component L_q^h according to (30). Since $-3pi_d i_q(\partial L_q/\partial\beta)/2$ in (8) contains a factor of $-3pi_d i_q/2$, the resultant L_q^h should be multiplied by this factor as shown in Fig. 5.

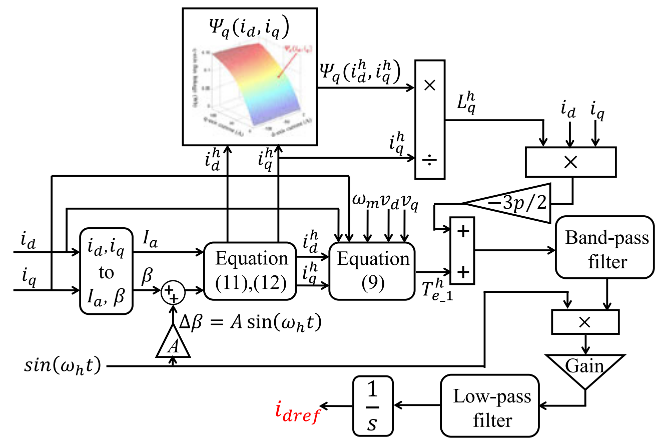

Fig. 5. Schematic of virtual signal injection blocks for the generation of the reference *d*-axis current ($i_{d\text{ref}}$).

Meanwhile, i_d^h and i_q^h calculated by (11) and (12) are also fed into (9) to calculate $T_{e\_1}^h$ together with the measured *d*- and *q*-axis currents, the measured motor speed, and the *d*- and *q*-axis command voltages. $T_{e\_1}^h$ and $(-3pi_d i_q/2)L_q^h$ are summed and processed by the bandpass filter whose center frequency equals to ω_h. The output of the bandpass filter is multiplied by $\sin(\omega_h t)$ and adjusted by a negative gain. The resultant signal is then processed by a low-pass filter and the output of the low-pass filter should be proportional to M which is given by (32)

$$M = \frac{\partial T_{e\_1}}{\partial\beta} - \frac{3p}{2}\frac{\partial L_q}{\partial\beta} i_d i_q = \frac{\partial T_e}{\partial\beta} - \text{error}_3 \tag{32}$$

$$\text{error}_3 = \text{error}_{\text{MTPA}} - \left(-\frac{3p}{2}\frac{\partial L_q}{\partial\beta} i_d i_q\right). \tag{33}$$

The output of the low-pass filter is fed to an integrator to adjust the reference *d*-axis current until M is equal to zero. As can be seen in Fig. 1, since the $\text{error}_{\text{MTPA}}$ is dominated by $-3pi_d i_q(\partial L_q/\partial\beta)/2$, the error_3 given by (33) should be much smaller than $\text{error}_{\text{MTPA}}$. Therefore, the MTPA control accuracy should be improved. It is worth noting that $3pi_q(\partial\Psi_m/\partial\beta)/2$ and $3pi_d i_q(\partial L_d/\partial\beta)/4$ in $\text{error}_{\text{MTPA}}$ can also be compensated in the similar way. However, this increases the complexity of the control scheme and requires more information about machine parameters while the improvement of the control accuracy may not be significant. The delay caused by the bandpass filter and low-pass filter in Fig. 5 can be minimized by the self-learning control described in [27].

Authorized licensed use limited to: ULAKBIM-UASL - Ahi Evran Universitesi. Downloaded on March 16,2022 at 12:48:36 UTC from IEEE Xplore. Restrictions apply.

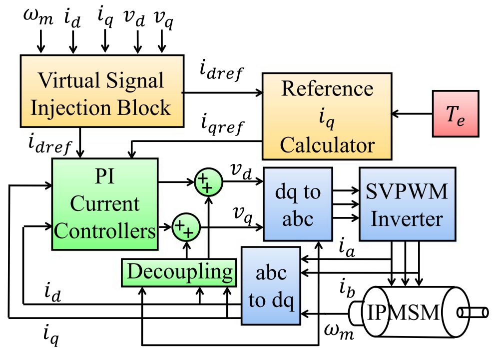

Fig. 6. Overall schematic of the IPMSM drive control system.

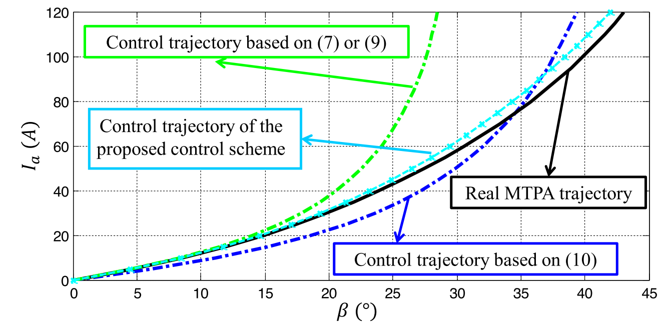

Fig. 7. Real MTPA trajectory and resultant control trajectories based on the first motor model and different MTPA control schemes.

TABLE II
PARAMETERS OF THE SECOND IPMSM MODEL

Number of pole-pairs	4
Phase resistance	13.27 mΩ
Maximum current	450 A
Peak power below base speed	80 kW
Base/maximum speed	2728/7000 r/min
Continuous/peak torque	109/280 N·m
Nominal *d*-axis inductance	0.187 mH
Nominal *q*-axis inductance	0.494 mH
Nominal permanent magnet flux linkage	84.93 mWb
Peak power at maximum speed	80 kW

The overall schematic of the IPMSM drive control system employing the proposed control scheme is shown in Fig. 6.

As shown in Fig. 6, the reference *d*-axis current is generated by the virtual signal injection scheme illustrated in Fig. 5. The resultant reference *d*-axis current together with the reference torque are fed to the reference *q*-axis current calculator to obtain the reference *q*-axis current ($i_{q\mathrm{ref}}$) based on (34). Since the generation of the reference *d*-axis current for MTPA operation is independent of the reference *q*-axis current, the motor parameters L_d, L_q, Ψ_m in the following equation can be assumed as their nominal values or obtained from predefined lookup tables:

$$i_{q\mathrm{ref}} = \frac{T_e}{\frac{3}{2}p\left[\Psi_m + (L_d - L_q)\, i_{d\mathrm{ref}}\right]}. \tag{34}$$

The resultant reference *d*- and *q*-axis currents will be compared with the measured *d*- and *q*-axis currents in proportional-integral (PI) current controllers to generate the reference *d*- and *q*-axis voltages after decoupling.

V. SIMULATION STUDIES

In this section, the performance of the proposed VSIC scheme illustrated in Figs. 5 and 6 will be studied by simulations. Since the characteristic of the $\mathrm{error}_{\mathrm{MTPA}}$ in (8) may vary with different motors, the simulations were performed based on two nonlinear IPMSM drive system models. The motor specifications of the two IPMSMs are given in Tables I and II, respectively. The $\Psi_q(i_d, i_q)$ in Fig. 4 is modeled as a fifth-order polynomial of *d*- and *q*-axis currents. Moreover, the MTPA control performances of the existing VSIC schemes based on (9) and (10) and the conventional MTPA control based on the mathematical models given by (6) and (7) are also simulated and compared with the simulation results of the proposed control scheme.

A. Simulations Based on the First IPMSM Model

Simulations were first performed based on a high fidelity nonlinear motor model [28] whose specification is given in Table I. The real MTPA trajectory, the resultant control trajectory based on (7) or (9), the resultant control trajectory based on (10), and the control trajectory generated by the proposed control scheme, in the form of I_a versus optimal β curves are compared in Fig. 7.

As can be seen in Fig. 7, the resultant control trajectory of the proposed control scheme is always close to the real MTPA trajectory. The small error between the control trajectory of the proposed control scheme and the real MTPA trajectory is due to the neglect of $3pi_q(\partial\Psi_m/\partial\beta)/2$ and $3pi_di_q(\partial L_d/\partial\beta)/4$ in (8).

However, the control trajectory calculated by (7) with the same machine parameters of the motor model leads to significant errors with respect to the real MTPA trajectory. These errors will definitely affect the MTPA control performance. The existing VSIC based on (9) generates same control trajectory as the trajectories calculated by (7), which also contains the relatively large errors. The error of the existing VSIC based on (10) is smaller than that of the virtual signal injection based on (9) when $I_a > 40$ A. This is due to the fact that $i_d\partial L_q/\partial\beta$ and $\partial\Psi_d/\partial\beta$ in (26) cancel each other partly. However, when 0 A $\leq I_a \leq 40$ A, the error of VSIC based on (10) is larger than that of the VSIC based on (9).

B. Simulations Based on the Second IPMSM Model

Simulations were also performed based on the second nonlinear IPMSM model whose specifications are given in Table II. The corresponding real MTPA trajectory, the resultant control trajectory based on (7) or (9), the resultant control trajectory based on (10), and the control trajectory generated by the proposed control scheme are illustrated in Fig. 8.

Again, the proposed control scheme tracks the real MTPA trajectory accurately. Moreover, as illustrated in Fig. 8, the error of the existing VSIC based on (9) is smaller than that of the VSIC based on (10) when $I_a \leq 200$ A, but the existing virtual signal injection based on (10) has better MTPA control accuracy when $I_a > 200$ A. Therefore, although the existing VSIC schemes

Authorized licensed use limited to: ULAKBIM-UASL - Ahi Evran Universitesi. Downloaded on March 16,2022 at 12:48:36 UTC from IEEE Xplore. Restrictions apply.

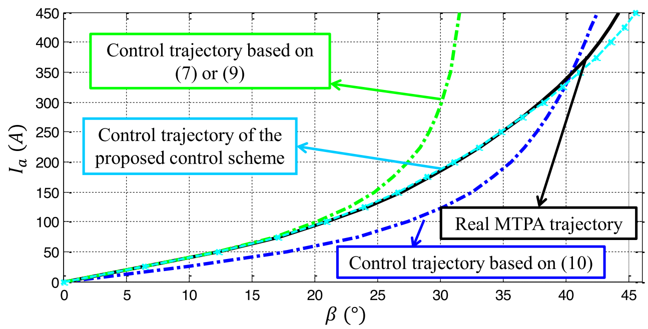

Fig. 8. Real MTPA trajectory and resultant control trajectories based on the second motor model and different MTPA control schemes.

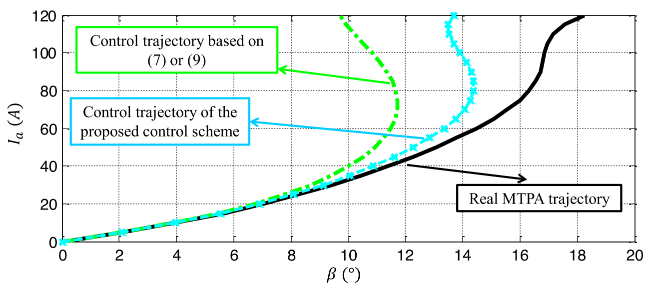

Fig. 9. Simulation results when saliency ratio is about 1.6.

based on (9) and (10) require less knowledge of machine parameters, their MTPA control performances vary with current amplitude and machine characteristics significantly. However, the proposed control scheme can always track the MTPA points with a relatively high accuracy.

C. Simulations With IPMSM Having Low Saliency Ratio

The two motor prototypes in this paper are specifically designed for electric vehicle (EV) tractions and their saliency ratios are typical for IPMSMs, i.e., between 2 and 3, for the purpose of high attainable reluctance torque. To represent the low saliency machines, L_q of the first IPMSM model whose parameters are given in Table I has been multiplied by 0.6 and the saliency ratio was reduced to about 1.6. The drives have been simulated, and the results are illustrated in Fig. 9.

As can be seen, the proposed scheme is much better than the control scheme based on (7) and (9). The maximum deviation from the real MTPA point is about 4° when proposed drive is employed. This deviation is caused by the neglected error terms, i.e., $3pi_q(\partial\Psi_m/\partial\beta)/2$ and $3pi_di_q(\partial L_d/\partial\beta)/4$ in $\text{error}_{\text{MTPA}}$, since these two error terms do not cancel each other exactly.

With a low salience ratio, the reluctance torque contribution is less significant. Hence, the MTPA point is less sensitive to β. Consequently, the small deviation in β will not result in a large difference in copper loss.

VI. Experimental Results

In order to verify the proposed control scheme, experiments were performed on a 10 kW prototype IPMSM drive system. The IPMSM whose specifications are given in Table I is mounted via a high precision inline torque transducer on the test-rig

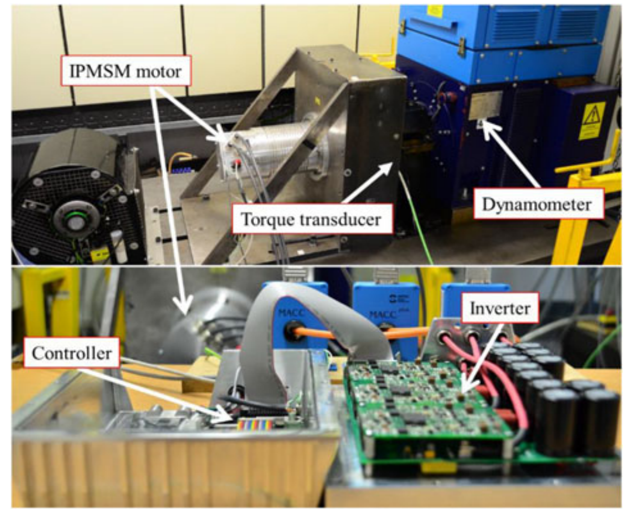

Fig. 10. Experimental test-rig.

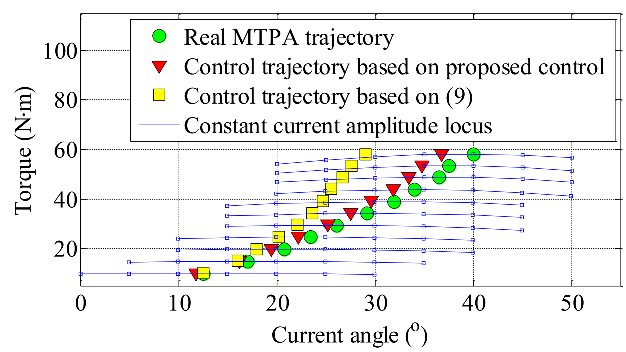

Fig. 11. Torque versus current angle of different resultant control trajectories when speed was 400 r/min.

and loaded by the dynamometer, as shown in Fig. 10. During the tests, the motor was controlled in torque control mode. $\Psi_q(i_d, i_q)$ given in (29) is modeled as a fifth-order polynomial of d- and q-axis currents. L_d in (9) is obtained from a lookup table which is generated based on FEA. In order to minimize the influences of the fundamental component and other harmonics on the output of the virtual signal injection, the frequency of the virtually injected signal should be as high as possible but the maximum frequency is limited by the sample rate of the controller. In this study, the frequency and amplitude of the virtually injected signal was set to 1000 Hz and 0.001 rad, respectively. The bandpass filter in Fig. 5 was designed to be of fourth order with a bandwidth of 1 Hz at the center frequency of the virtually injected signal.

A. MTPA Points Tracking Test

Tests were first performed to track the MTPA points when the motor speed was 400 r/min and the reference torque varied from 5 to 60 N·m in steps of 5 N·m. Fig. 11 shows the real MTPA points obtained by curve-fitting of the constant current amplitude locus, the control trajectory based on the proposed control scheme and the control trajectory based on virtual signal injection without the compensation of the derivative terms, i.e.,

Authorized licensed use limited to: ULAKBIM-UASL - Ahi Evran Universitesi. Downloaded on March 16,2022 at 12:48:36 UTC from IEEE Xplore. Restrictions apply.

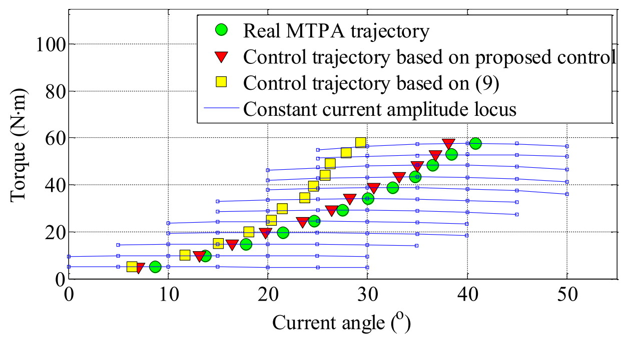

Fig. 12. Torque versus current angle of different resultant control trajectories when speed was 1000 r/min.

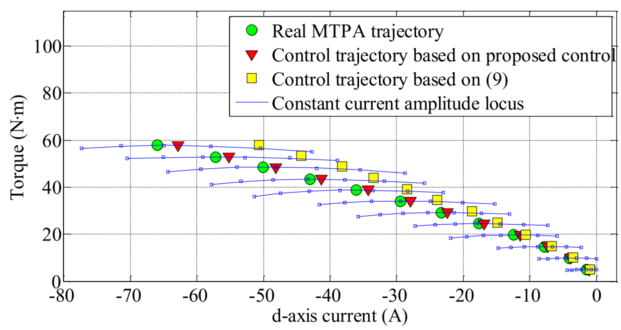

Fig. 13. Torque versus current angle of different resultant control trajectories when speed was 1000 r/min.

the VSIC based on (9). As can be seen in Fig. 11, due to the $\mathrm{error}_{\mathrm{MTPA}}$ in (8), the resultant control trajectory of the existing virtual signal injection MTPA control based on (9) contained large errors and the MTPA control scheme based on (7) suffered from the similar problem even if the parameters used were accurate. However, the proposed control scheme compensated the $-3pi_d i_q(\partial L_q/\partial\beta)/2$ term in $\mathrm{error}_{\mathrm{MTPA}}$ and the control accuracy was significantly increased. The relatively small error between the control trajectory of the proposed control scheme and the real MTPA trajectory was caused by a combination of the measurement error and the error in the $\Psi_q(i_d, i_q)$ model as well as the error due to neglecting $3pi_q(\partial\Psi_m/\partial\beta)/2$ and $3pi_d i_q(\partial L_d/\partial\beta)/4$ terms.

Experiments were also performed when speed was 1000 r/min with reference torque varied from 5 to 60 N·m in steps of 5 N·m. The resultant control trajectories of the proposed control scheme and the existing virtual signal injection based on (9) are compared with the real MTPA trajectory shown in Fig. 12. Again, the proposed control scheme compensated the $\mathrm{error}_{\mathrm{MTPA}}$ effectively and its performance is independent of motor speed when voltage saturation is not reached [22].

The torque versus d-axis current trajectories plotted in Fig. 12 are shown in Fig. 13. As can be seen, the neglect of $\mathrm{error}_{\mathrm{MTPA}}$ also caused large errors in the resultant d-axis currents and this error is significantly compensated by the proposed control scheme. The relatively small errors between the real MTPA trajectory and the resultant trajectory of the proposed control scheme may be caused by the error in $\Psi_q(i_d, i_q)$ and the neglect of $3pi_q(\partial\Psi_m/\partial\beta)/2$ and $3pi_d i_q(\partial L_d/\partial\beta)/4$ in $\mathrm{error}_{\mathrm{MTPA}}$.

TABLE III
COMPARISON OF THE CURRENT AMPLITUDE

Torque reference (N·m)	Current amplitude of the proposed control scheme (A)	Current amplitude of the control scheme based on (9) (A)	Difference (%)
60	101.14	104.40	3.2
55	92.48	95.310	3.1
50	83.99	86.32	2.8
45	75.58	77.12	2.0
40	67.25	68.31	1.6
35	58.97	59.56	1.0
30	50.63	51.13	1.0
25	42.37	42.57	0.5
20	34.06	34.14	0.2
15	25.70	25.74	0.2
10	17.25	17.28	0.2
5	8.71	8.71	0.0

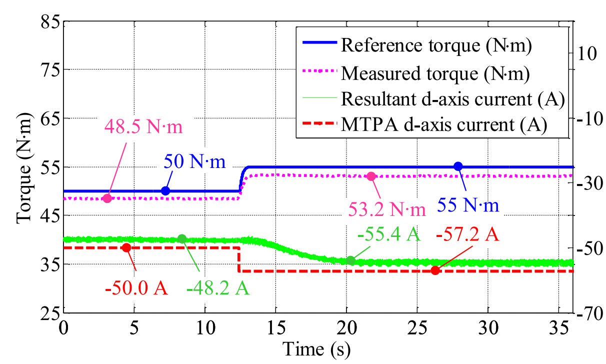

Fig. 14. Response of d-axis current to a step change in torque reference at speed of 1000 r/min.

However, since the constant current amplitude loci are smooth and flat around the MTPA points, the relatively small errors will not cause much additional copper loss.

As mentioned in Section IV, the reference q-axis current is calculated by (34) based on reference torque. Therefore, if the output torque of the proposed control scheme and the control scheme based on (9) is the same, the resultant current magnitude will be different. Table III compares the current amplitudes of the two different control schemes when the torque is varied from 5 to 60 N·m and speed is kept at 1000 r/min. As can be seen, when the torque is low, the difference between the two control schemes is very small. The difference becomes noticeable when the torque is greater than 30 N·m. At 60 N·m, the difference reach 3.2% which implies that the proposed control would lead to ∼6.4% reduction in copper loss compared to the control scheme based on (9).

B. Performance During Payload Torque Changes

In order to illustrate the performance of the proposed control scheme during payload torque changes, the response of d-axis current to a step change in torque command from 50 to 55 N·m at speed of 1000 r/min is shown in Fig. 14. The measured torque and the MTPA d-axis currents are also shown in Fig. 14. It can be seen that with the proposed control scheme the d-axis current tracks the MTPA d-axis currents automatically and the resultant

Authorized licensed use limited to: ULAKBIM-UASL - Ahi Evran Universitesi. Downloaded on March 16,2022 at 12:48:36 UTC from IEEE Xplore. Restrictions apply.

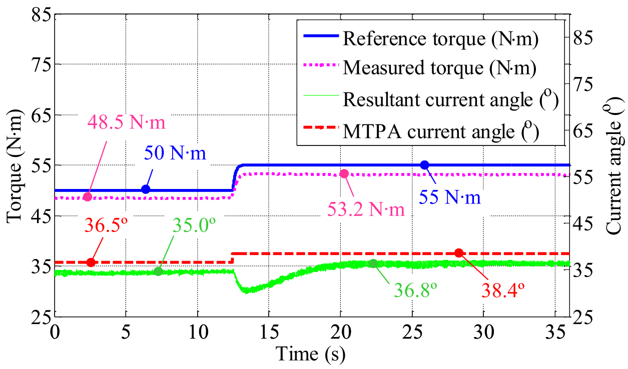

Fig. 15. Response of current angle to a step change in torque reference at speed of 1000 r/min.

d-axis current is very close to the MTPA d-axis current. The small error will not cause much additional copper loss because the constant current amplitude loci shown in Fig. 13 are flat around the MTPA points. The small error between the measured and reference torques may be caused by the combined effect of the errors of machine parameters in (34) and the friction torque which is not accounted in the torque reference.

The resultant current angle with the same operation conditions of Fig. 14 is shown in Fig. 15. Due to the step change of reference torque, the q-axis current increases, which results in initial decrease in the current angle. However, the proposed control scheme adjusts the current angle until it is close to the MTPA current angles.

VII. Conclusion

In this paper, the influence of the derivatives of machine parameters with respect to current angle on MTPA operation was analyzed. A virtual signal injection based control scheme has been proposed to compensate the errors for MTPA operation due to the derivative terms, and its performance has been validated by experiments. The MTPA control accuracies of the conventional model based MTPA control schemes, the existing VSIC schemes, and the proposed control scheme were compared. It has been shown that although the existing virtual signal injection based MTPA control schemes require less knowledge of machine parameters, their MTPA control performance vary significantly with current amplitude and machine characteristics. However, the proposed control scheme can always track the MTPA points with a relatively high accuracy. The limitation of the proposed control scheme is that it requires the knowledge of Ψ_q as a function of d- and q-axis currents and inaccurate $\Psi_q(i_d, i_q)$ may affect the MTPA control accuracy.

References

[1] H. Zhou, W. Zhao, G. Liu, R. Cheng, and Y. Xie, "Remedial field-oriented control of five-phase fault-tolerant permanent-magnet motor by using reduced-order transformation matrices," *IEEE Trans. Ind. Electron.*, vol. 64, no. 1, pp. 169–178, Jan. 2017. doi: 10.1109/TIE.2016.2599501.

[2] T. Inoue, Y. Inoue, S. Morimoto, and M. Sanada, "Mathematical model for MTPA control of permanent-magnet synchronous motor in stator flux linkage synchronous frame," *IEEE Trans. Ind. Appl.*, vol. 51, no. 5, pp. 3620–3628, Sep./Oct. 2015. doi: 10.1109/TIA.2015.2417128.

[3] S. Morimoto, K. Hatanaka, Y. Tong, Y. Takeda, and T. Hirasa, "High performance servo drive system of salient pole permanent magnet synchronous motor," in *Proc. IEEE Ind. Appl. Soc. Annu. Meeting*, Sep./Oct. 1991, pp. 463–468. doi: 10.1109/IAS.1991.178196.

[4] S. Morimoto, M. Sanada, and Y. Takeda, "Wide-speed operation of interior permanent magnet synchronous motors with high-performance current regulator," *IEEE Trans. Ind. Appl.*, vol. 30, no. 4, pp. 920–926, Jul./Aug. 1994. doi: 10.1109/28.297908.

[5] T. Sun, J. Wang, and M. Koc, "Self-learning direct flux vector control of interior permanent magnet machine drives," *IEEE Trans. Power Electron.*, vol. 32, no. 6, pp. 4652–4662, Jun. 2017. doi: 10.1109/TPEL.2016.2602243.

[6] T. M. Jahns, G. B. Kliman, and T. W. Neumann, "Interior permanent-magnet synchronous motors for adjustable-speed drives," *IEEE Trans. Ind. Appl.*, vol. IA-22, no. 4, pp. 738–747, Jul. 1986. doi: 10.1109/TIA.1986.4504786.

[7] A. Consoli, G. Scarcella, G. Scelba, and A. Testa, "Steady-state and transient operation of IPMSMs under maximum-torque-per-ampere control," *IEEE Trans. Ind. Appl.*, vol. 46, no. 1, pp. 121–129, Jan./Feb. 2010. doi: 10.1109/TIA.2009.2036665.

[8] S.-Y. Jung, J. Hong, and K. Nam, "Current minimizing torque control of the IPMSM using ferrari's method," *IEEE Trans. Power Electron.*, vol. 28, no. 12, pp. 5603–5617, Dec. 2013. doi: 10.1109/TPEL.2013.2245920.

[9] R. S. Colby and D. W. Novotny, "An efficiency-optimizing permanent-magnet synchronous motor drive," *IEEE Trans. Ind. Appl.*, vol. 24, no. 3, pp. 462–469, May/Jun. 1988. doi: 10.1109/28.2897.

[10] S. Bolognani, L. Peretti, and M. Zigliotto, "Online MTPA control strategy for DTC synchronous-reluctance-motor drives," *IEEE Trans. Power Electron.*, vol. 26, no. 1, pp. 20–28, Jan. 2011. doi: 10.1109/TPEL.2010.2050493.

[11] R. Antonello, M. Carraro, and M. Zigliotto, "Maximum-torque-per-ampere operation of anisotropic synchronous permanent-magnet motors based on extremum seeking control," *IEEE Trans. Ind. Electron.*, vol. 61, no. 9, pp. 5086–5093, Sep. 2014. doi: 10.1109/TIE.2013.2278518.

[12] S. Kim, Y.-D. Yoon, S.-K. Sul, and K. Ide, "Maximum torque per ampere (MTPA) control of an IPM machine based on signal injection considering inductance saturation," *IEEE Trans. Power Electron.*, vol. 28, no. 1, pp. 488–497, Jan. 2013. doi: 10.1109/TPEL.2012.2195203.

[13] G. Liu, J. Wang, W. Zhao, and Q. Chen, "A novel MTPA control strategy for IPMSM drives by space vector signal injection," *IEEE Trans. Ind. Electron.*, vol. 64, no. 12, pp. 9243–9252, Dec. 2017. doi: 10.1109/TIE.2017.2711507.

[14] J. Lee, K. Nam, S. Choi, and S. Kwon, "Loss-minimizing control of PMSM with the use of polynomial approximations," *IEEE Trans. Power Electron.*, vol. 24, no. 4, pp. 1071–1082, Apr. 2009. doi: 10.1109/TPEL.2008.2010518.

[15] Y. A.-R. I. Mohamed and T. K. Lee, "Adaptive self-tuning MTPA vector controller for IPMSM drive system," *IEEE Trans. Energy Convers.*, vol. 21, no. 3, pp. 636–644, Sep. 2006. doi: 10.1109/TEC.2006.878243.

[16] G. Schoonhoven and M. N. Uddin, "MTPA and FW based robust nonlinear speed control of IPMSM drive using lyapunov stability criterion," *IEEE Trans. Ind. Appl.*, vol. 52, no. 5, pp. 4365–4374, Sep./Oct. 2016. doi: 10.1109/TIA.2016.2564941.

[17] M. N. Uddin and M. M. I. Chy, "Online parameter-estimation-based speed control of PM AC motor drive in flux-weakening region," *IEEE Trans. Ind. Appl.*, vol. 44, no. 5, pp. 1486–1494, Sep./Oct. 2008. doi: 10.1109/TIA.2008.926205.

[18] D. Q. Dang, M. S. Rafaq, H. H. Choi, and J.-W. Jung, "Online parameter estimation technique for adaptive control applications of interior PM synchronous motor drives," *IEEE Trans. Ind. Electron.*, vol. 63, no. 3, pp. 1438–1449, Mar. 2016. doi: 10.1109/TIE.2015.2494534.

[19] A. Shinohara, Y. Inoue, S. Morimoto, and M. Sanada, "Direct calculation method of reference flux linkage for maximum torque per ampere control in DTC-based IPMSM drives," *IEEE Trans. Power Electron.*, vol. 32, no. 3, pp. 2114–2122, Mar. 2016. doi: 10.1109/TPEL.2016.2569140.

[20] T. Sun, J. Wang, and M. Koc, "On accuracy of virtual signal injection based MTPA operation of interior permanent magnet synchronous machine drives," *IEEE Trans. Power Electron.*, vol. 32, no. 9, pp. 7405–7408, Sep. 2017. doi: 10.1109/TPEL.2016.2638020.

[21] T. Sun, J. Wang, and M. Koc, "Virtual signal injection based direct flux vector control of IPMSM drives," *IEEE Trans. Ind. Electron.*, vol. 63, no. 8, pp. 4773–4782, Aug. 2016. doi: 10.1109/TIE.2016.2548978.

[22] T. Sun, J. Wang, and X. Chen, "Maximum torque per ampere (MTPA) control for interior permanent magnet synchronous machine drives based on virtual signal injection," *IEEE Trans. Power Electron.*, vol. 30, no. 9, pp. 5036–5045, Sep. 2015. doi: 10.1109/TPEL.2014.2365814.

Authorized licensed use limited to: ULAKBIM-UASL - Ahi Evran Universitesi. Downloaded on March 16,2022 at 12:48:36 UTC from IEEE Xplore. Restrictions apply.

[23] Y. Zhao, "Virtual square-wave current injection based maximum torque per ampere control for interior permanent-magnet synchronous machines," in *Proc. IEEE Transp. Electrific. Conf. Expo.*, Jun. 2016, pp. 1–6. doi: 10.1109/ITEC.2016.7520289.

[24] T. Inoue, Y. Inoue, S. Morimoto, and M. Sanada, "Maximum torque per ampere control of a direct torque controlled PMSM in a stator flux linkage synchronous frame," *IEEE Trans. Ind. Appl.*, vol. 52, no. 3, pp. 2360–2367, May/Jun. 2016. doi: 10.1109/TIA.2016.2531618.

[25] Y.-C. Kwon, S. Kim, and S.-K. Sul, "Six-step operation of PMSM with instantaneous current control," *IEEE Trans. Ind. Appl.*, vol. 50, no. 4, pp. 2614–2625, Jul./Aug. 2014. doi: 10.1109/TIA.2013.2296652.

[26] T. Sun and J. Wang, "Extension of virtual signal injection based MTPA control for interior permanent magnet synchronous machine drives into field weakening region," *IEEE Trans. Ind. Electron.*, vol. 62, no. 11, pp. 6809–6817, Nov. 2015. doi: 10.1109/TIE.2015.2438772.

[27] T. Sun, J. Wang, M. Koc, and X. Chen, "Self-learning MTPA control of interior permanent magnet synchronous machine drives based on virtual signal injection," *IEEE Trans. Ind. Appl.*, vol. 52, no. 4, pp. 3062–3070, Jul./Aug. 2016. doi: 10.1109/TIA.2016.2533601.

[28] X. Chen, J. Wang, B. Sen, P. Lazari, and T. Sun, "A high-fidelity, computationally efficient model for interior permanent magnet machines considering the magnetic saturation, spatial harmonics and iron loss effect," *IEEE Trans. Ind. Electron.*, vol. 62, no. 7, pp. 4044–4055, Jul. 2015. doi: 10.1109/TIE.2014.2388200.

Tianfu Sun (S'15–M'16) was born in China. He received the B.Eng. degree in mechanical engineering and M.Sc. degree in civil engineering from the Dalian University of Technology, Dalian, China, in 2009 and 2012, respectively, and the Ph.D. degree in electrical and electronic engineering from the University of Sheffield, Sheffield, U.K., in 2016.

From 2016 to 2017, he was with the Department of Electronic and Electrical Engineering, University of Sheffield, where he was a Postdoctoral Research Fellow. He is currently an Associate Professor of electric drives with the Shenzhen Institutes of Advanced Technology, Chinese Academy of Sciences, Shenzhen, China. His current research interests include power electronics and motor drives.

Mikail Koç was born in Turkey. He received the B.Sc. degree from ESOGU University, Eskisehir, Turkey, in 2009, the M.Sc. degree from Nottingham University, Nottingham, U.K., in 2012, and the Ph.D. degree from the University of Sheffield, Sheffield, U.K., in 2016, all in electrical and electronic engineering.

He is currently an Assistant Professor with Ahi Evran University, Kirsehir, Turkey. His research interests include advanced control strategies for ac drives.

Jiabin Wang (S'94–A'96–M'01–SM'03) received the B.Eng. and M.Eng. degrees from the Jiangsu University of Science and Technology, Zhenjiang, China, in 1982 and 1986, respectively, and the Ph.D. degree from the University of East London, London, U.K., in 1996, all in electrical and electronic engineering.

He is currently a Professor of electrical engineering with the University of Sheffield, Sheffield, U.K. From 1986 to 1991, he was with the Department of Electrical Engineering, Jiangsu University of Science and Technology, where he was appointed a Lecturer in 1987 and an Associated Professor in 1990. He was a Postdoctoral Research Associate with the University of Sheffield, from 1996 to 1997, and a Senior Lecturer with the University of East London from 1998 to 2001. His research interests range from motion control and electromechanical energy conversion to electric drives for applications in automotive, renewable energy, household appliances, and aerospace sectors.

Dr. Wang is a Fellow of the IET.

Authorized licensed use limited to: ULAKBIM-UASL - Ahi Evran Universitesi. Downloaded on March 16,2022 at 12:48:36 UTC from IEEE Xplore. Restrictions apply.